ELSEVIER

Generation of quasiperiodic oscillations in pairs of coupled maps

Paulo C. Rech [a,b], Marcus W. Beims [b,*], Jason A.C. Gallas [a,c]

[a] *Departamento de Física, Universidade do Estado de Santa Catarina, 89223-100 Joinville, Brazil*
[b] *Departamento de Física, Universidade Federal do Paraná, 81531-990 Curitiba, Brazil*
[c] *Instituto de Física, Universidade Federal do Rio Grande do Sul, 91501-970 Porto Alegre, Brazil*

Abstract

We investigate analytically the emergence of quasiperiodic and mode-locked states of *arbitrary* period in pairs of coupled maps. Quasiperiodic and mode-locked states arise from Naimark–Sacker bifurcations and exhibit very rich local dynamics. We determine analytically both states for pairs of maps under symmetric and asymmetric couplings. Lyapunov spectra, portraits in parameter-space and in phase-space are used to show the transition from quasiperiodic and from mode-locked states into chaotic states and to check the range of validity of the approximations implicit in the standard normal forms.
© 2006 Elsevier Ltd. All rights reserved.

1. Introduction

The behavior of orbits near a Naimark–Sacker (NS) bifurcation [1,2] reveals many interesting features about the motion of particles in complex systems. Fixed-point solutions are transformed into quasiperiodic states or limit cycles after the bifurcation. In other words, particles starting in a steady state (or even a mode-locked or synchronized state) end up moving in cycles around one or more centers. Such transformation are observed, for example, when vortex structures appear in fluid dynamics [3,4], or in the solutions of multi-agent models of biological swarming [5]. Examples of such transitions emerging from NS bifurcations can also be mentioned: nonlinear beam oscillations excited by lateral force in sound and vibration physics [6], the Euler method applied to delay differential equation [7], in the pattern formation and oscillations in a system of self-regulating cells in neural science [8], the collapse of predator populations in biology [9] and applications in monetary economies [10]. Two coupled maps may exhibit the above-mentioned motion. Since they are two-dimensional dynamical systems, they might be able to reproduce the spatially extended properties of quasiperiodic motion on a limit cycle. This makes the study of the emergence of synchronized and quasiperiodic states in two coupled maps, and also its transition to desynchronized states, a very actual problem, as corroborated by recent works [11]. A pair of coupled maps is the model considered in this paper.

---

* Corresponding author. Tel.: +55 41 361 3467; fax: +55 41 361 3418.
 E-mail address: mbeims@fisica.ufpr.br (M.W. Beims).

In practical applications it is very difficult to determine model parameters which lead to a desirable solution. In order to obtain them, a complete determination of stability regions in the parameter space is necessary. This can be a difficult task since multi-stability is a common phenomenon in complex systems and the nonlinearity of the models makes it impossible to find general analytic solutions. In order to overcome such problems, numerical methods have been used [12] to determine periodic orbits and their stability regions in parameter space. Analytical results for stability boundaries in the parameter space are only possible for relatively low periods [13], nowadays of the order of 11 [14,15]. One may also resort to an analytical method, the classic method of the resultants [16,17], where the symmetry of the eigenvalues may be used to split the characteristic polynomial of the Jacobian matrix into two coupled polynomials, which allows to find stability regions for Hopf bifurcations in parameter space. Another way to overcome the above-mentioned problems is to search for metric properties or similarities in the parameter space. A well-known example is the observation by Feigenbaum that for many one-parameter families of scalar maps, as one follows a cascade of period-doubling bifurcations in parameter space, the ratio of distances between successive period-doubling parameter values tends to approach a limiting ratio independent of the family maps [18]. Another example is the existence of self-similar shapes in the parameter space of two-parameters maps [19,20]. In some cases, it is possible to find a linear transformation that brings the stability region of a orbit with a given period of *one* map very close to the stability region for a fixed point from *another* map [19]. Therefore, informations of stability regions in the parameter space may be obtained by proper transformations or metric properties.

The purpose of this paper is to determine analytically and numerically the emergence of quasiperiodic and mode-locked states (or synchronized states) in pairs of coupled maps. Using normal forms, analytical results are obtained near NS bifurcations where, as will be seen, a rich local dynamics emerges. Although the model considered here presents a very complex dynamics in the parameter space, simple expressions are obtained for the location, in parameter space, where quasiperiodic and mode-locked states of *arbitrary* period are generated. Moreover, numerical results including Lyapunov exponents, phase space and parameter space portraits are used to describe the transition of mode-locked and quasiperiodic states into chaotic states.

In order to apply our results to a wide range of different nonlinear dynamical systems, coefficients of a normal form will be derived for two generic classes of couplings: the first one, a *nonlinear asymmetric* coupling between the maps is assumed, and for the second one, a *linear* and *symmetric* coupling is used. The prototype of the first class is given by

$$x_{t+1} \equiv h_1^a(x_t, y_t) = a - py_t^2 - qx_t^2, \tag{1}$$

$$y_{t+1} \equiv h_2^a(x_t, y_t) = x_t, \tag{2}$$

where x_t, y_t are the variables, a, p and q the parameters, and t represents the discrete time ($t = 0, 1, 2, \ldots$). The above model [21] is rich to describe transitions between degenerated routes to chaos expected to occur in physical systems. The parameters p and q allow a convenient tuning between the relative influence of the terms they control. The parameter a controls the nonlinearity of the quadratic map. Some parameters of the normal form for the NS bifurcation have been derived for an asymmetric coupled map in the context of oscillating memories [22].

The other considered case is the linear symmetric coupling, given by

$$x_{t+1} \equiv h_1^s(x_t, y_t) = a - x_t^2 + b(x_t - y_t), \tag{3}$$

$$y_{t+1} \equiv h_2^s(x_t, y_t) = a - y_t^2 + b(y_t - x_t), \tag{4}$$

where a is the nonlinear parameter from the uncoupled maps and b represents the coupling strength between them. In this model, both quadratic maps are uncoupled if points lie on the diagonal $y_t = x_t$, and coupled for off-diagonal points ($y_t \neq x_t$). The diagonal $y_t = x_t$ is called the synchronization line and does not exist in the asymmetric case. Although there are many works [23] describing aspects of the dynamics of two maps coupled symmetrically, the determination of parameters of the normal forms for a NS bifurcation has not been done yet.

In Section 2, necessary and sufficient conditions to for the occurrence of a NS bifurcation and its corresponding normal form are reviewed briefly. Sections 3 and 4 consider the asymmetric and symmetric cases, respectively. In both cases, coefficients of the normal forms are determined for the NS bifurcations and analytical expressions for the location in the parameter space of mode-locked states are derived. Numerical calculations are done and the transition from mode-locked and quasiperiodic states into chaotic states is demonstrated. Some concluding remarks are given in Section 5.

2. The normal form

A powerful method to describe analytically the local properties of complex systems near bifurcations points, is the determination of normal forms [1,24–26]. In general, for each bifurcation type (Pitchfork, Naimark–Sacker, etc.), a spe-

cific normal form has to be derived. Once the normal form is determined for the bifurcation, all physical models have the same normal form for that kind of bifurcation. The coefficients of the normal forms, however, change from model to model. For example, the normal form for a Pitchfork bifurcation [24] is the same for different systems, but its coefficients will be different and they depend on particular properties of the system. The determination of the coefficients of normal forms is a laborious work, but it gives essential information about the dynamics of the system near the bifurcation point.

In this section, we consider the normal form for the NS bifurcation. Additional details may be found in [1,24–26]. Although the derivation of the normal form itself is not complicate, formulas for the determination of its coefficients are not simple. These formulas are written here explicitly and they are valid for any dynamical system which suffers a NS bifurcation. Essentially four steps are necessary to determine the coefficients.

2.1. Translation to the origin

Normal forms are derived on the central manifold [24]. To translate the coordinates (x, y) of the dynamical systems [Eqs. (1) and (2) or, Eqs. (3) and (4)] to the central manifold coordinates (u, v), the following transformation is necessary

$$\begin{pmatrix} u \\ v \end{pmatrix} = M \begin{pmatrix} x - x_1 \\ y - y_1 \end{pmatrix}. \tag{5}$$

Here (x_1, y_1) is the position of the fixed point, and M is the 2×2 transformation matrix. The columns of M are the eigenvectors associated to the eigenvalues λ, calculated from the Jacobian matrix of the original system in (x, y) coordinates. The above transformation translates the bifurcating equilibrium point to the origin and brings the linear part into the normal form.

If we write $\lambda = e^{+ic}$ and $\bar{\lambda} = e^{-ic}$, the linear part of the (any) dynamical system can be put in the form

$$\begin{pmatrix} u \\ v \end{pmatrix} \mapsto \begin{bmatrix} \cos(c) & -\sin(c) \\ \sin(c) & \cos(c) \end{bmatrix} \begin{pmatrix} u \\ v \end{pmatrix}, \tag{6}$$

where the constant c, calculated at the bifurcation point, is determined from

$$c = \arctan \frac{\Im[\lambda]}{\Re[\lambda]}. \tag{7}$$

The notation $\Re[z]$ and $\Im[z]$ means to take the real and imaginary part of the complex number z, respectively. The overbar denotes complex conjugation. The nonlinear part from the dynamical system is added to Eq. (6), i.e.,

$$\begin{pmatrix} u \\ v \end{pmatrix} \mapsto \begin{bmatrix} \cos(c) & -\sin(c) \\ \sin(c) & \cos(c) \end{bmatrix} \begin{pmatrix} u \\ v \end{pmatrix} + \begin{bmatrix} f(u, v) \\ g(u, v) \end{bmatrix}. \tag{8}$$

In this equation, the linear part in u and v is separated from the nonlinear part in $f(u, v)$ and $g(u, v)$.

2.2. NS bifurcation conditions

By definition [1,24–26], the NS bifurcation will occur if the conditions

$$|\lambda_{1,2}(a_{NS})| = 1, \quad \text{but} \tag{9}$$

$$\lambda_{1,2}^j(a_{NS}) \neq 1 \quad \text{for } j = 1, 2, 3, 4, \tag{10}$$

$$\frac{d}{da}(|\lambda_{1,2}(a_{NS})|) = d \neq 0, \tag{11}$$

are satisfied. Here, $\lambda_{1,2}$ are the eigenvalues of the Jacobian matrix, a_{NS} is the bifurcation parameter calculated at the bifurcation point, and d is a constant. Note that the above conditions relate to the linearized system only, and they suffice to conclude that the NS bifurcation occurs. However, to determine coefficients of the normal form and details about the bifurcation, the nonlinear terms from Eq. (8) have to be analyzed. In order to do this, functions $f(u, v)$ and $g(u, v)$ are expanded in a series.

2.3. Expansion

It is adequate to rewrite Eq. (8) in the complex plane by using the transformation $z = u + iv$. After this transformation, Eq. (8) results in

$$z \mapsto \lambda z + f(z, \bar{z}) + \mathrm{i}g(z, \bar{z}). \tag{12}$$

This expression is exactly the dynamical system written in the complex plane and with the bifurcation point located at the origin. Expanding $f(z, \bar{z}) + \mathrm{i}g(z, \bar{z})$ in a Taylor expansion in z and $\bar{z}$, we obtain

$$z \mapsto \lambda z + \tfrac{1}{2}\xi_{20}z^2 + \xi_{11}z\bar{z} + \tfrac{1}{2}\xi_{02}\bar{z}^2 + \tfrac{1}{2}\xi_{21}z^2\bar{z} + \cdots. \tag{13}$$

Higher order term are neglected. The coefficients of this expansion are related to $f(u,v)$ and $g(u,v)$ by

$$\xi_{20} = \tfrac{1}{8}[f_{uu} - f_{vv} + 2g_{uv} + \mathrm{i}(g_{uu} - g_{vv} - 2f_{uv})], \tag{14}$$

$$\xi_{11} = \tfrac{1}{4}[f_{uu} + f_{vv} + \mathrm{i}(g_{uu} + g_{vv})], \tag{15}$$

$$\xi_{02} = \tfrac{1}{8}[f_{uu} - f_{vv} - 2g_{uv} + \mathrm{i}(g_{uu} - g_{vv} + 2f_{uv})], \tag{16}$$

$$\xi_{21} = \tfrac{1}{16}[f_{uuu} + f_{uvv} + g_{uuv} + g_{vvv} + \mathrm{i}(g_{uuu} - g_{uvv} - f_{uuv} - f_{vvv})], \tag{17}$$

where f_{uv} means $(\partial^2 f/\partial u\,\partial v)(0,0)$, etc.

2.4. Obtaining the normal form

At this point, the dynamical system is written as an expansion [Eq. (13)] around the bifurcation point. This expansion however, may not have the simplest possible form. In order to find the simplest form, which also keeps all local relevant information near the bifurcation point, the transformation $\eta = \eta(z) = z + \mathrm{O}(|z|^2)$ is used to bring Eq. (13) in the following normal form in the complex plane:

$$\eta \mapsto \lambda\eta + l\eta^2\bar{\eta} + \mathrm{O}(|\eta|^5), \tag{18}$$

with l being a complex number determined by

$$l = \left[\frac{(1 - 2\lambda)\bar{\lambda}}{\lambda - 1}\xi_{11}\xi_{20} - \frac{|\xi_{11}|^2}{(1 - \lambda^3)\bar{\lambda}} - \frac{2|\xi_{02}|^2}{(1 - \lambda)\bar{\lambda}} + \xi_{21} \right].$$

Substituting $\lambda = \mathrm{e}^{\mathrm{i}\theta}$, and $\eta = r\mathrm{e}^{\mathrm{i}\phi}$ in Eq. (18), and after some straightforward calculations, the right hand side of (18) transforms into

$$r\left(1 + \Re[\bar{\lambda}l]r^2\right)\mathrm{e}^{\mathrm{i}\left(\theta + \phi + \Im[\bar{\lambda}l]r^2\right)}. \tag{19}$$

The radial and angular parts are the normal forms in polar coordinates, which can be written in a more general form as [24]

$$r_{t+1} = r_t\left[1 + d(a - a_{\mathrm{NS}}) + er_t^2\right], \tag{20}$$

$$\theta_{t+1} = \theta_t + c + sr_t^2, \tag{21}$$

where c, d, e and s are the coefficients of the normal form. The coefficient d is determined from Eq. (11), $c = \phi$ from (7), and comparing Eqs. (20) and (21) with (19), we obtain

$$e = \Re[\bar{\lambda}l] \quad \text{and} \quad s = \Im[\bar{\lambda}l]. \tag{22}$$

The constants d, c, e and s determine the properties and stability of solutions near the NS bifurcation. If the condition $e \neq 0$ is satisfied, then there is a limit cycle in the surroundings of a_{NS}. The stability of this cycle is determined by the sign of e. If $e < 0$, then the limit cycle is stable and the bifurcation is called supercritical, otherwise, the limit cycle is unstable and the bifurcation is subcritical.

The normal forms (20) and (21) are able to reproduce the local property of solutions near NS bifurcations, which is necessary for the purpose of this paper. As we will see later in details, these normal forms describe the transition from fixed-point solutions (of any period) into mode-locked or quasiperiodic solutions. Higher order terms could be included in Eqs. (20) and (21), but they only give information about details of the solutions near the bifurcation point. At the end of Section 3 it will be explained more about these details.

Summarizing, in order to determine completely the normal form, it is necessary to calculate the functions $f(u,v)$ and $g(u,v)$, and determine the coefficients d, c, s and e of Eqs. (20) and (21), as described in this section. This will be done in next sections for the asymmetric and symmetric models, respectively.

3. The asymmetric coupling

The quasiperiodic oscillations shown in this paper are generated inside a rich and complex dynamics in parameter space. The dynamics in the surroundings of the quasiperiodic oscillations is responsible for details of these oscillations, like radius of the limit cycles, frequency of mode-locked states, and even the chaotic motion. An appropriate and efficient way to get informations about all these complex motions, as the parameters are changed, is to study stability domains in the parameter space. The asymmetric model of Eqs. (1) and (2) contains three parameters a, p and q. Since it is not easy to analyze a three-dimensional parameter space, two particular cases will be considered. For the first one (Section 3.1), the parameter $p = 1$ is kept fixed while a and q are varied. For the second one (Section 3.2), $q = 1$ is considered, while a and p may change.

In order to understand the difference between both particular cases, some comments are needed. The parameters a and q control, respectively, the nonlinearity of the coupled logistic map of Eq. (1) in two different ways: (a) the *translation* of the point x by an amount of a. For each iteration in Eq. (1), the new values of x are translated by the constant a; and (b) *dilatation* of the point x^2 by an amount of q. For each time step, the values of x^2 in Eq. (1) are multiplied by q. Keeping this in mind, Section 3.1 analyzes the dynamics as the coupling strength between maps is constant ($p = 1$) and the nonlinearity may change via translation and dilatation of coordinates. In Section 3.2 otherwise, the dynamics will be analyzed as dilatation is kept fixed ($q = 1$) while coupling strength and nonlinearity due translation are changed.

Fig. 1 shows the isoperiodic diagrams [27] for both cases. For each figure the discretized parameter interval is a mesh of 500×350 points. Both diagrams show the complexity of alternation between stability domains. Different stability domains can be distinguished by tonalities. The white region indicates the parameters which lead to quasiperiodic motion near the boundary C, and chaotic motion far away from C. If the parameter are chosen to be in the gray region, the motion in the phase space has an attractor at infinity. Different regions of periodicity are identified by integer numbers which indicate the period of that region.
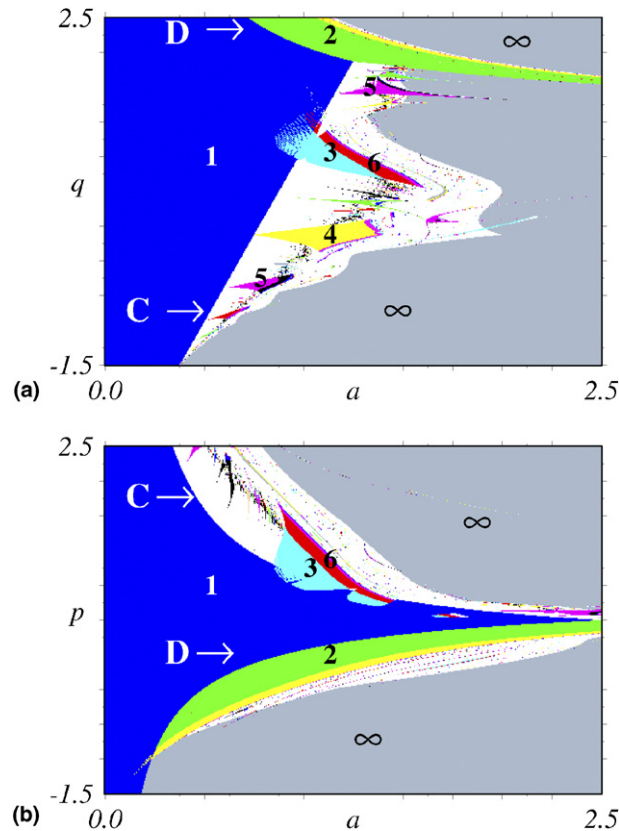

Fig. 1. Stability domains in the parameter space for the map of Eqs. (1) and (2). The numbers indicate the periods: (a) case $p = 1$; (b) case $q = 1$.

The region of period-1 has two boundaries marked as D and C. Period doubling 1×2^n bifurcation is found after the boundary D, while near (to the right) the boundary C, a very complex dynamics is found. There is a sequence of periodic regions embedded in the quasiperiodic region. Not all of these periodic regions can be observed clearly for the scale shown in Fig. 1. Exceptions are the three periodic structures (two periods 5 and one period 4) which are born exactly on the line C of Fig. 1(a). Both, periodic and quasiperiodic motion, are born exactly on the line C.

3.1. p = 1, q and a arbitrary

Numerical and analytical results for the case $p = 1$ will be presented firstly. The fixed points of period-1 are $M_1 \equiv (x_1, x_1)$, which is stable in region 1 of Fig. 1(a), and $M_2 \equiv (x_2, x_2)$, which is unstable in the same region. The values of $x_{1,2}$ are

$$x_{1,2} = \frac{-1 \pm \sqrt{1 + 4a(1 + q)}}{2(q + 1)}, \tag{23}$$

which are real for $a \geqslant (-1)/[4(1 + q)]$. The eigenvalues of the Jacobian matrix are given by

$$\lambda_{1,2} = -qx \pm \sqrt{(qx)^2 - 2y}, \tag{24}$$

which can assume real or complex conjugate values, depending on the sign of $(qx)^2 - 2y$. In order to study the stability of a specific orbit, it is necessary to substitute (x, y) by the related values of $x_{1,2}$ from Eq. (23).

Starting with real eigenvalues and considering the point M_1, it is possible to obtain the bifurcation points of period-1 by making $\lambda_1 = 1$ or $\lambda_2 = 1$. The resulting line is

$$q = -\frac{1 + 4a}{4a}, \tag{25}$$

which is a curve on the parameter space where a stable period-1 orbit is born. This curve is not shown in Fig. 1(a). Using $\lambda_1 = -1$ or $\lambda_2 = -1$, we get

$$q = \frac{3 + 8a + \sqrt{9 + 32a}}{8a}, \tag{26}$$

which defines a curve in the parameter space where a bifurcation $1 \to 2$ from the fixed point M_1 occurs. This is the curve which defines the doubling boundary D of Fig. 1(a), and is the first curve of the sequence of curves related with the 1×2^n period doubling bifurcations.

The complex conjugates eigenvalues are given by

$$\lambda = -qx + i\sqrt{-(qx)^2 + 2y}, \tag{27}$$

$$\bar{\lambda} = -qx - i\sqrt{-(qx)^2 + 2y}. \tag{28}$$

For the point M_1, the first NS condition $|\lambda| = |\bar{\lambda}| = 1$ (see Eq. (9)) leads to $q = 4a - 3$, which is exactly the straight line which defines the boundary C of Fig. 1(a). The solution of this equation, i.e.,

$$a \equiv a_{NS} = (q + 3)/4, \tag{29}$$

defines the bifurcation boundary. The coefficient $d = 1/(2 + q)$ is determined from Eqs. (11) and (27), and is greater than zero for $q > -2$. With these informations, it is possible to observe that the NS bifurcation conditions (described in Section 2) are satisfied, and Eq. (29) is called the NS line. In order to calculate the coefficient e from Eq. (20), it is necessary to translate the bifurcation point to the origin of a new coordinate system given by

$$(\hat{x}, \hat{y}) = (x - x_1, y - y_1). \tag{30}$$

The eigenvectors corresponding to λ and $\bar{\lambda}$ (these are calculated on the NS line) are, respectively, given by

$$\frac{1}{2}\begin{pmatrix} -q + i\chi \\ 2 \end{pmatrix} \quad \text{and} \quad \frac{1}{2}\begin{pmatrix} -1 - i\chi \\ 2 \end{pmatrix},$$

where $\chi = \sqrt{(2 - q)(2 + q)}$. In order to separate the linear part from the nonlinear part, as in Eq. (8), a new basis is introduced which allows the transformation

$$\begin{pmatrix} u \\ v \end{pmatrix} = \frac{1}{\chi} \begin{pmatrix} q & 2 \\ \chi & 0 \end{pmatrix} \begin{pmatrix} \hat{x} \\ \hat{y} \end{pmatrix}.$$

Rewriting Eqs. (1) and (2) in this new coordinate system, transforming it into the complex plane [as for Eq. (12)], it is easy to obtain the nonlinear terms of the map

$$f(u,v) = \frac{-q\chi^2 u^2 + 2q^2 \chi uv - q^2(1+q)v^2}{4\chi},$$

$$g(u,v) = \left(-1 + \frac{q^2}{4}\right)u^2 + \frac{q}{2}\chi uv - q\left(1 + \frac{q}{4}\right)v^2.$$

With these functions, the coefficients e and s can be determined from Eq. (22), and they are

$$e = -\frac{3 + 2q + q^2 + 4q^3 + 4q^4 + q^5}{4(2+q)}, \tag{31}$$

$$s = -\frac{\chi(q^7 + 3q^6 - 2q^5 - 9q^4 + q^3 + 3q^2 - 11q - 2)}{4(q+2)^2(q-2)(q-1)}. \tag{32}$$

The coefficient e is always negative for $q > -2$, as it can be observed in Fig. 2(a). The limit cycle is therefore stable for these values of q. From the results obtained for e and d, it is possible to conclude that the fixed point M_1 suffers a NS bifurcation along the line (29) in the parameter space. All conditions for a NS bifurcation reviewed in Section 2 are satisfied and the limit cycle, which exist for $a > a_{NS}$ [i.e., on the right hand side of the line C from Fig. 1(a)], is stable.

The local dynamics described by the normal forms (20) and (21) is very rich. It is possible, for example, to obtain informations related to the radius of the limit cycle and the rotation number. Making $r_{t+1} = r_t = r$ in Eq. (20), the radius of the limit cycle is determined by

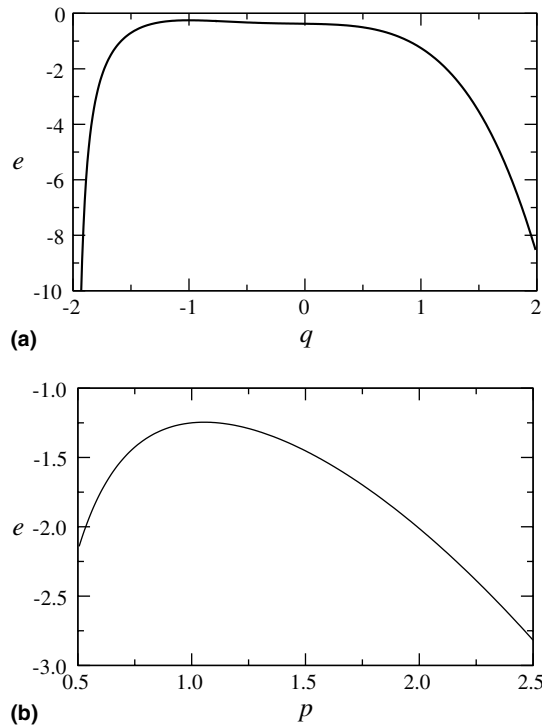$$r = \sqrt{-\frac{d}{e}(a - a_{NS})}. \tag{33}$$

(a)

(b)

Fig. 2. (a) Coefficient e from the normal form (21) as a function of the parameter q and (b) the same coefficient, but as a function of the parameter p calculated in Section 3.2. Since $e < 0$ in the considered q and p intervals, the limit cycles are stable in the same intervals.

Observe that r is always real because the limit cycles only exist for $a > a_{NS}$, $d > 0$ and $e < 0$.

Substituting r from Eq. (33) in Eq. (21), the rotation number on the limit cycle can be obtained from

$$\theta_{t+1} = \theta_t + \alpha(a), \tag{34}$$

where

$$\alpha(a) = c + sr^2 = c - \frac{sd}{e}(a - a_{NS}). \tag{35}$$

For points on the Naimark–Sacker line C ($a = a_{NS}$), results that $\alpha_c = c$, where c, obtained from Eq. (7) is

$$c = -\arctan \frac{\chi}{q} = -\arctan \sqrt{\frac{4}{q^2} - 1}, \tag{36}$$

with $-2 \leqslant q \leqslant 2$. It can be observed from the map (34), that for rational values of $\alpha_c/2\pi$, points on the limit cycle will be repeated, leaving to periodic points. For irrational values of $\alpha_c/2\pi$, points on the limit cycle will never repeat. Therefore, two cases have to be considered, depending on the ratio $\alpha_c/2\pi$:

(1) Mode-locking: If $\alpha_c/2\pi = m/n$ is a rational number, a periodic regime is obtained. In this case, a mode-locked state or synchronization is obtained, with n being the period of the orbit and m its multiplicity.
(2) Quasiperiodicity: If $\alpha_c/2\pi$ is an irrational number, the motion is quasiperiodic.

Regions of mode-locked states in the plane (a, q) can be observed in Fig. 1(a). They are identified with integer numbers n and are embedded in regions of quasiperiodicity. These periodic regions are similar to Arnold tongues structures observed in the circle map [4]. The points on the boundary C, where the tongues are born, can be obtained *analytically* by using

$$\alpha_c = c = -\arctan \frac{\chi}{q}. \tag{37}$$

This relation allows us to locate periodic mode-locked state (on the curve C) with *any* desirable period n. By choosing a period-n (and multiplicity m) and substituting $\alpha_c/2\pi = m/n$ in (37), the value of q can be determined from

$$q = -\frac{\chi}{\tan\left(2\pi \frac{m}{n}\right)}. \tag{38}$$

The parameter a is then obtained from Eq. (29).

Once the location of the period-n mode-locked states on the line C is found, it is possible to determine the stability boundaries (the Arnold tongues [4]) for values of $a > a_{NS}$, i.e., to the right of line C. In order to obtain such stability boundaries, it is necessary to introduce higher order terms in the normal forms (20) and (21) and, to repeat the calculations described above. For each period-n mode-locked state the derivation has to be repeated. This is a long work and will not be done in this paper. Such calculations are interesting for specific applications.

Eq. (37) agrees with numerical results. For example, the period-5 mode-locked region, clearly visible in the lower part of Fig. 1(a), is located at the parameters $(a, q) = (0.5955, -0.6180)$. The corresponding values of $\alpha_c/2\pi$ is 1/5. Notice that, since q is limited to ($-2 \leqslant q \leqslant 2$), only values of $\alpha_c/2\pi$ satisfying $-1/4 \leqslant \alpha_c/2\pi \leqslant 1/4$, are allowed. Fig. 3 shows the (a) bifurcation diagram and (b) behavior of the maximal Lyapunov exponent, h, for $0.5 < a < 1.25$ and $q = -0.3$. Different motions can be observed, namely, for negative exponents (periodic motion), zero exponent (quasiperiodic states) and positive exponent (chaotic motion with some windows of mode-locked states where $h < 0$). The arrow in Fig. 3(b) indicates the range of quasiperiodic motion which begins at the NS bifurcation point $(a, q) = (0.675, -0.3)$, where a fixed-point solution is transformed into a quasiperiodic motion. By increasing the value of a, the quasiperiodic motion exist until the chaotic motion is reached ($h > 0$). In the quasiperiodic region, the bifurcation diagram is filled out. For both Figures, the a axis was divided in 1000 points, the trajectories were initialized at $(x_0, y_0) = (0.1234, 0.5)$, and plotted after a transient of 200,000. For the bifurcation diagram, 60 points were plotted for each value of a.

Alternatively, trajectories in the phase space are used to observe the dynamics near the boundary C of Fig. 1(a). Fig. 4(a) shows four trajectories in the phase space for different values of a, while keeping $q = -0.3$. For $a = 0.68$, which is close to the NS bifurcation boundary C, an elliptic curve (limit cycle) with quasiperiodic motion is observed. This elliptic curve is deformed more and more as we move away (to the right) from the boundary C [see $a = 0.78, 0.88$ in Fig. 4(a)], until the chaotic attractor is reached at $a = 0.94$, with a Lyapunov exponent equal to 0.00989. In fact, trajectories move around the origin remembering a vortex like motion. As the chaotic attractor is reached, the curve is
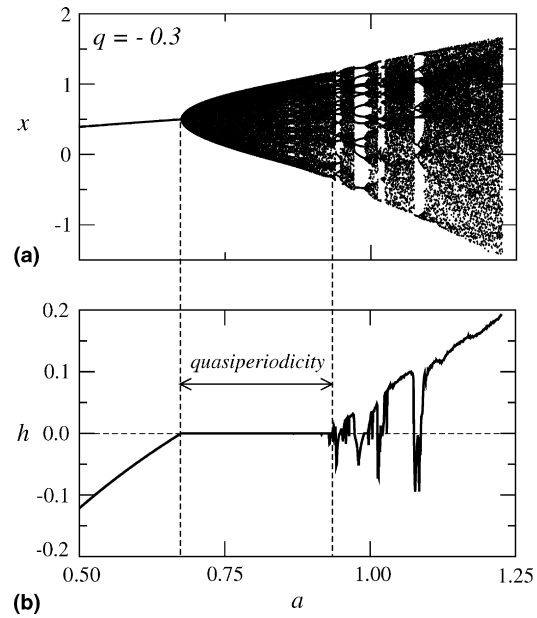
Fig. 3. (a) Bifurcation diagram and (b) maximal Lyapunov exponent for $q = -0.3$. The arrow shows the range of quasiperiodic motion.
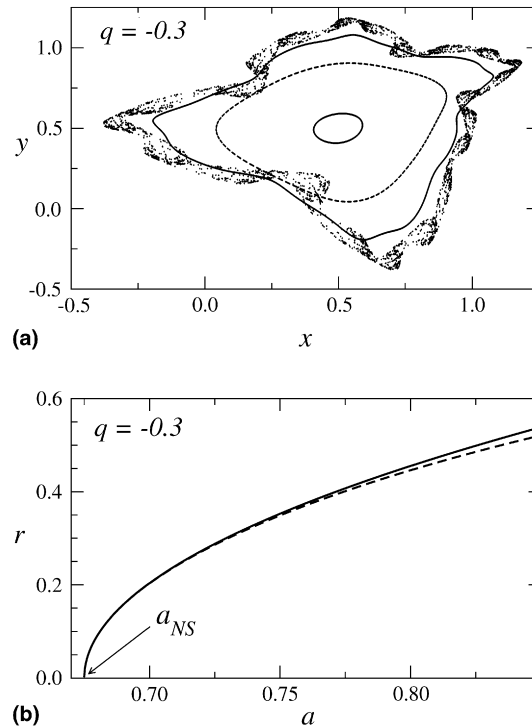

Fig. 4. Shown are: (a) four trajectories in the phase space with $q = -0.3$ and $a = 0.68, 0.78, 0.88, 0.94$ (chaotic state), from inside to outside and, (b) radius of the limit cycle as a function of the bifurcation parameter a, obtained analytically (dashed line) from Eq. (33) and numerically (solid line). Here $a_{NS} = 0.675$.
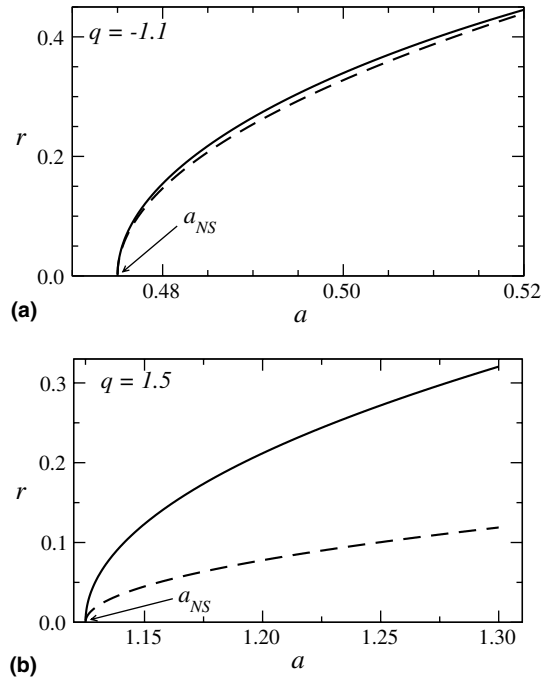
Fig. 5. Radius of the limit cycle as a function of the bifurcation parameter a, obtained analytically (dashed line) from Eq. (33) and numerically (solid line) for (a) $q = -1.1$, $a_{NS} = 0.475$ and (b) $q = 1.5$, $a_{NS} = 1.125$.

more and more complicated. Initial conditions and transient used for Fig. 4(a), are the same of those from Fig. 3. Each phase space trajectory of Fig. 4(a) was constructed with 5000 points.

Results obtained from the normal form are valid only locally near the bifurcation point. It is possible to compare analytical limit cycles, obtained from Eq. (33), with numerical results. Numerically we calculate the radius of the limit cycles and, as the chaotic region is approached, where the limit cycle is deformed, the radius is an average radius over all points of the trajectory. Fig. 4(b) compares the radius of the limit cycle calculated from Eq. (33) (dashed line) with the radius obtained by numerical simulations (solid line). Both curves are plotted as a function of the bifurcation parameter a and for $q = -0.3$. They agree very well for values starting close to the NS bifurcation point $a_{NS} = 0.675$ until $a \sim 0.73$. Only for values $a > 0.73$ both curves start to separate from each other. Therefore, the dynamics obtained from normal forms describes locally very well the numerical simulations. Other examples of the agreement between numerical (solid line) and local analytical (dashed line) approximations for the radius of the limit cycle are shown in Fig. 5. For $q = -1.1$ [shown in Fig. 5(a)], both lines agree in the whole range of a values. For $q = 1.5$ [see Fig. 5(b)] the agreement between numerical and analytical results decreases very fast. The reason for this can be explained as follows. A closer inspection of Fig. 1(a) shows that the interval in a, where the quasiperiodic motion exist in the parameter space, is larger for $q = -1.1$ than for $q = 1.5$. Far away from the NS bifurcation, when the chaotic region is approached, limit cycles are totally deformed [see Fig. 4(a)] and the numerical calculation of the limit cycle radius is worse. Since the chaotic state is reached "faster" (i.e., in a smaller a interval) for $q = 1.5$ than for $q = -1.1$, the limit cycles is deformed faster and, as a consequence, the agreement between analytical and numerical radius gets faster worse.

3.2. $q = 1$, p and a arbitrary

In this subsection, coefficients of the normal forms are determined for the case $q = 1$, a and p arbitrary. There is only one stable fixed point of period-1 in region 1 of Fig. 1(b), given by $N_1 \equiv (x_1, x_1)$, where

$$x_1 = \frac{-1 + \sqrt{1 + 4a(1+p)}}{2(p+1)}. \tag{39}$$

The eigenvalues of the Jacobian matrix are obtained by substituting $x = y = x_1$ in

$$\lambda_{1,2} = -x \pm \sqrt{x^2 - 2py}. \tag{40}$$

Considering only complex conjugated eigenvalues for the point N_1, the condition $|\lambda| = |\bar{\lambda}| = 1$ leads to

$$p = \frac{3 + \sqrt{9 + 16a}}{8a}, \tag{41}$$

which is the boundary C of Fig. 1(b) and the NS bifurcation line. The coefficients of the normal forms from Eqs. (20) and (21) can also be obtained in this case. In order to do this, we use the same procedure as in last subsection. From Eq. (7), follows

$$c = -\arctan \chi' = -\arctan \sqrt{4p^2 - 1}. \tag{42}$$

From the condition (11) we obtain

$$d = \frac{p\sqrt{p}}{2p + 1}. \tag{43}$$

From this equation we observe that d is real and different from zero if $p > 0$. As a consequence, $d > 0$ and the NS bifurcation condition (11) is satisfied. The parameter which determines the stability of the limit cycle is obtained from (22)

$$e = -\frac{1 + 4p + 4p^2 + p^3 + 2p^4 + 3p^5}{4p^2(2p + 1)}, \tag{44}$$

which is negative for values $p > -1/2$ or $p > 1/2$. Since p must be greater then zero in order to keep d real, only values of $p > 1/2$ are of interest. In order to obtain a stable limit cycle, it is necessary that $e < 0$, and the NS bifurcation will be supercritical. Fig. 2(b) is a plot of e as a function of p. It clearly shows that $e < 0$ for the plotted range.

The last parameter s can be determined also from (22)

$$s = \frac{2p^7 + 11p^6 - 3p^5 - p^4 + 9p^3 + 2p^2 - 3p - 1}{4\chi'(2p + 1)p^2(p - 1)}. \tag{45}$$

The functions $f(u,v)$ and $g(u,v)$ are in this case

$$f(u,v) = \frac{\chi'^2 u^2 - 2\chi' uv + (1 + 4p)v^2}{-4p\chi'},$$

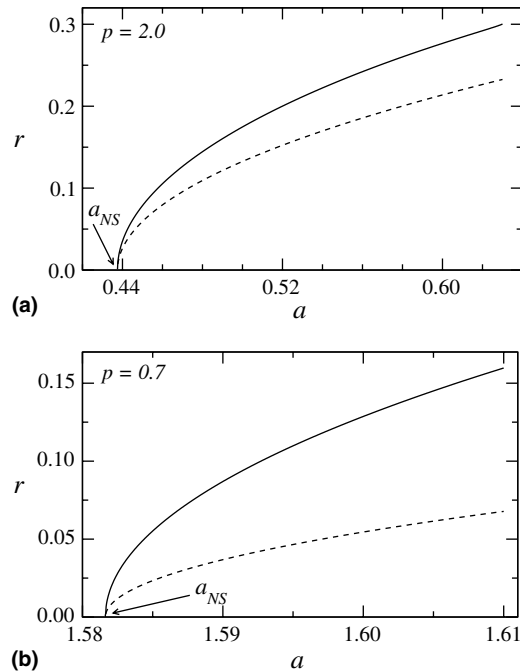$$g(u,v) = \frac{\chi'^2 u^2 - 2\chi' uv + (1 + 4p)v^2}{-4p}.$$

Fig. 6. Radius of the limit cycle as a function of the bifurcation parameter a, obtained analytically (dashed line) and numerically (solid line) for (a) $p = 2.0$ and $a_{NS} = 0.4375$ and (b) $p = 0.7$ and $a_{NS} = 1.5816$.

These results allows us to conclude that the NS bifurcation occurs on the line C from Fig. 1(b), for $p \geqslant 1/2$. The radius of the stable limit cycle can also be determined from Eq. (33), and the rotation number is given by

$$\alpha_c = c = -\arctan \chi'. \tag{46}$$

With this relation, it is possible to determine the exact location, on the parameter space, where a mode-locked state of any period-n is born. The condition $p \geqslant 1/2$, combined with Eq. (46), results in $-1/4 \leqslant \alpha_c/2\pi \leqslant 0$, which defines the allowed interval of values of $\alpha_c/2\pi$.

Fig. 6 compares the radius of the limit cycle (dashed line) with the radius obtained by numerical simulations (solid line) for two values of p. The agreement is better for the case $p = 2.0$, shown in Fig. 6(a), if compared with the case $p = 0.7$, shown in Fig. 6(b). Also here the agreement still depends how fast the chaotic region in reached as the parameter a increases.

The analytic evolution of the limit cycles can be obtained again from Eq. (33) and (34). Two kind of motions appear also in this case, depending on the ratio $\alpha_c/2\pi = m/n$: the *mode-locked motion* if $\alpha_c/2\pi$ is a rational number, and the *quasiperiodic motion* if $\alpha_c/2\pi$ is irrational. As in last subsection, numerical simulations for space phase trajectories, bifurcation diagrams, and Lyapunov spectra were also realized here. From the qualitative point of view, such simulations do not add any new informations if compared with results from last subsection. For this reason, these simulations are not shown here.

4. The symmetric coupling

The situation is very different for the symmetric model described by Eqs. (3) and (4). The coupling is linear and the states of both maps are uncoupled along the diagonal $x_t = y_t$, called also the synchronization line. Since it is not possible to obtain a limit cycle along a one-dimensional line, NS bifurcation are not expected to occur along the synchronization line. Moreover, the existence of the diagonal line and the symmetric coupling, implies that all off-diagonal fixed points appear in pairs, located symmetrically on each side of the diagonal. It was shown [28] that there exist four period-1 orbits for the symmetric coupling. Two fixed points of them are on the diagonal, and the others are off-diagonal. The off-diagonal are unstable and, as a consequence, cannot suffer a NS bifurcation. Therefore, period-1 fixed point does not suffer a NS bifurcation in the symmetric model. This assert was checked by doing the linear stability analysis for the period-1 orbits. This analysis will not be shown here since it is not relevant for the NS bifurcation. In order to find fixed points which undergoes a NS bifurcation, we analyzed orbits with period-2.

It was shown [28] that for the dynamical system described by Eqs. (3) and (4), two kinds of period-2 orbits appear. One of them is born through period doubling on the diagonal $x_t = y_t$. The other one, which will be considered here, is born from the bifurcation $1 \rightarrow 2$ along the line $4a - 4b^2 - 3 - 8b = 0$. This line in the parameter space separates stability domains of period-1 and period-2, and is obtained analytically by a linear stability analysis (for more details, see [28]). The fixed points of this period-2 orbit have the following property:

$$\cdots (x_1, x_2) \rightarrow (x_2, x_1) \rightarrow (x_1, x_2) \cdots, \tag{47}$$

where

$$x_{1,2} = \frac{2b+1}{2} \pm \frac{\sqrt{-4b^2 + 4a - 8b - 3}}{2}. \tag{48}$$

If the curve inside the square root of (48) is not zero, then $x_1 \neq x_2$ and the period-2 fixed points are off-diagonal. The eigenvalues of the Jacobian matrix for this period-2 orbit are

$$\lambda_{1,2} = 6b^2 + 10b - 4a + 4 \pm 2b\sqrt{5b^2 + 10b - 4a + 4}. \tag{49}$$

Applying the condition $|\lambda_1| = |\lambda_2| = 1$ leads to

$$4b^2 + 10b - 4a + 5 = 0, \tag{50}$$

which is the NS bifurcation line. It is easy to show that $d = 4$, $\lambda_{1,2}^j(a_{NS}, b) \neq 1$ for $j = 1, 2, 3, 4$, and that

$$c = \arctan \frac{2b\eta}{2b^2 - 1}, \tag{51}$$

where $\eta = \sqrt{(1-b)(1+b)}$.

Using the same procedure as in last section, the functions $f(u, v)$ and $g(u, v)$ can be determined, and from them, the coefficients e and s. All functions and coefficients are presented in Appendix A. Details of calculations will not be
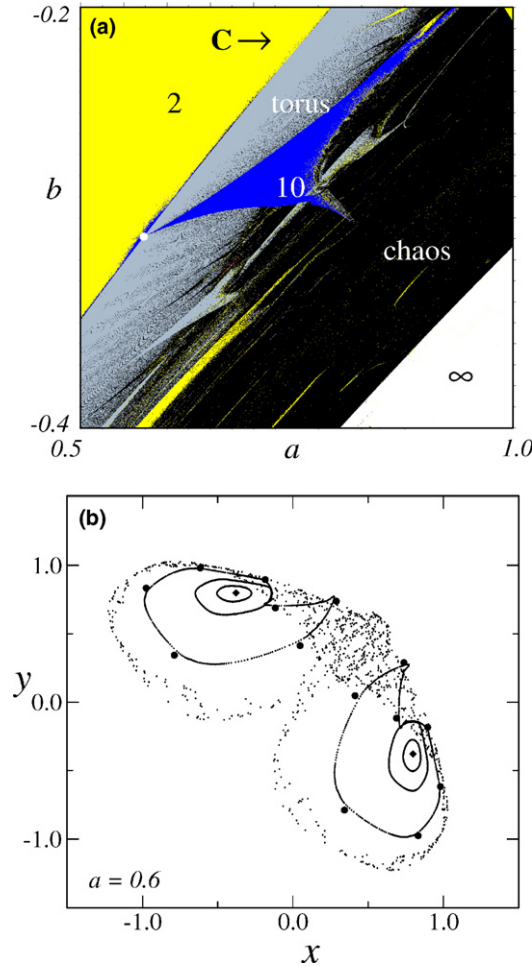
Fig. 7. (a) Stability domains in the parameter space for the map of Eqs. (3) and (4). The numbers indicate the periods. (b) Six trajectories in the phase space for $a = 0.6$ and $b = -0.29$ (fixed points of period-2, see diamonds), -0.30, -0.32, -0.38, -0.384 (phase-locked state of period-14, see black circles), and -0.417 (chaotic state), from inside to outside.

repeated here. Once the coefficients of the normal form are determined, then the local maps (20) and (21) can be studied. The analytic evolution of the limit cycles can be obtained again from Eq. (33) and (34), but using the parameter d, e, s and c from the symmetric problem. Two kinds of motion appear also in this case, depending on the ratio $\alpha(a)/2\pi = c = m/n$: the *mode-locked motion* if $\alpha_c/2\pi$ is a rational number, and the *quasiperiodic motion* if $\alpha_c/2\pi$ is irrational.

As in the asymmetric case, there are many period-n mode-locked regions embedded in the quasiperiodic region. Examples of stability domains in the parameter space are shown in Fig. 7(a). Different stability domains can be distinguished by tonalities and the numbers indicate the period. Line C is the NS bifurcation line, Eq. (50), where the quasiperiodic and mode-locked states are born. One mode-locked state of period-10 is observed embedded in the region of quasiperiodicity. The values of the parameters, where a mode-locking motion with any period-n is born, can be determined analytically using results obtained by the normal form. Substituting c from Eq. (51) in Eq. (35), it is possible to get

$$\alpha_c = \arctan \frac{2b\eta}{2b^2 - 1} = \frac{m}{n}. \tag{52}$$

By choosing $m = 1$ and $n = 10$, for example, and using Eqs. (52) and (50), the pair (a, b) can be determined and the location of the period-10 mode-locked state (on the line C) of Fig. 7(a) is exactly known. The result is $(a, \text{b}) = (0.5730, -0.3090)$, and is marked as a white point in Fig. 7(a).

Different from the asymmetric coupling considered in last section, here *two* limit cycles are born at the NS line from Eq. (50), one for each of the period-2 fixed points [Eq. (48)]. These fixed points can be seen in the phase space shown in Fig. 7(b) (see the diamonds) inside the inner circles (ellipsis). The location in the parameter space is $(a, b) = (0.6, -0.29)$. In this figure, 1000 points were used after a transient of 50,000 from the initial condition $(x_0, y_0) = (0.1234, 0.5)$. Keeping $a = 0.6$ fixed, six trajectories in the phase space are shown for different values of b between -0.29 (period-2 region), and
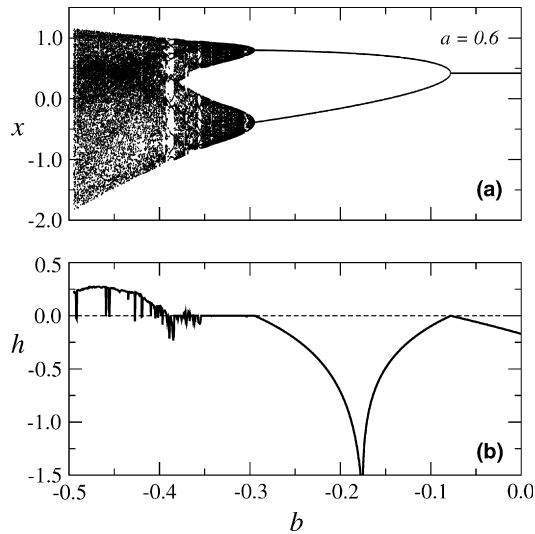

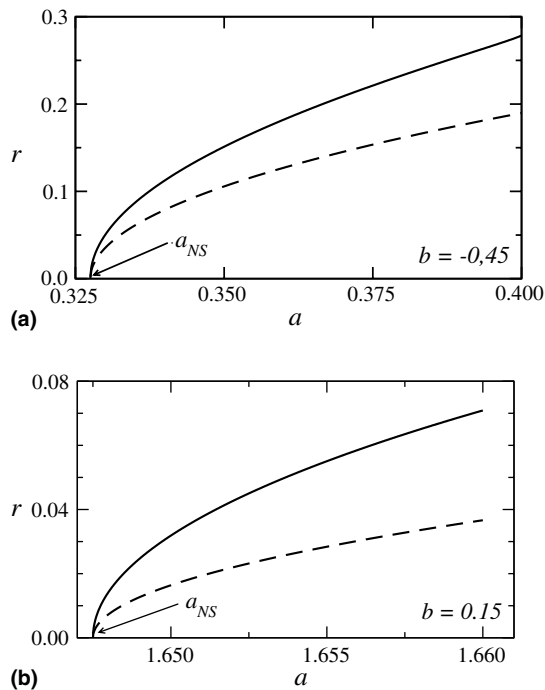Fig. 8. (a) Bifurcation diagram and (b) maximal Lyapunov exponent.

Fig. 9. Radius of the limit cycle as a function of the bifurcation parameter a, obtained analytically (dashed line) from Eq. (33) and numerically (solid line) for (a) $b = -0.45$ and $a_{NS} = 0.3275$ and (b) $b = 0.15$ and $a_{NS} = 1.6475$.

−0.417 (chaotic region). It can be observed that for $b = -0.29$, only two off-diagonal fixed points exist, each on one side of the diagonal (diamond points inside the inner ellipsis). As the value of b decreases to −0.30, the NS line from Eq. (50) is crossed, and both fixed points are transformed into two limit cycles (ellipsis surrounding fixed points). As the value of b decreases more and more, the limit cycle start to blow up ($b = -0.30, -0,32$), then its elliptic form is deformed ($b = -0.38$), a mode-locked state of period-14 appears at $b = -0.384$ [see the 14 black circles in Fig. 7(b)], and finally a chaotic state is generated at $b = -0.417$.

The above transition from quasiperiodic to chaotic motion can be confirmed in Fig. 8, which presents the bifurcation diagram and the maximal Lyapunov exponent for $a = 0.6$, and b changing from 0.0 (period-1 region) to −0.5 (chaotic region). By decreasing b, a period doubling bifurcation $1 \rightarrow 2$ occurs firstly. At $b = -0.29$ [Lyapunov exponent $h = 0$, see Fig. 8(b)], a NS bifurcation occurs and both fixed points are transformed into limit cycles (ellipsis). After this, the ellipsis are deformed and, at $b = -0.384$, a period-14 mode-locked *stable* state emerges. Decreasing the value of b more and more, the chaotic state is reached as the value of h is greater than zero. Depending on parameter combination, it is also possible to find the emergence of limit-cycles, which are born from the NS line, but from fixed points with higher periods. As one example, the emergence of *four* limit-cycles, and its transition to a chaotic motion, was found along the line $b = 0.25$ and a between 1.2 and 1.48.

Fig. 9 compares the radius of the limit cycle calculated from Eq. (33) (dashed line) with the radius obtained by numerical simulations (solid line). Curves are plotted as a function of the bifurcation parameter a and for different values of b. Fig. 9(a) shows results for $b = -0.45$ while Fig. 9(b) for $b = 0.15$. In both cases, we observe that the normal form approximation is valid only locally.

5. Conclusions

A common phenomenon in nature is that particles, starting from a fixed point and induced by some external influence, may exhibit a vortex structures [3,4] or begin to move around one or more centers [5]. Such phenomenon certainly depends on the parameters which control the system, like for example, intensity of the external influence, temperature, viscosity in case of fluids, etc. Usually these systems are very complex, their dynamics is not simple and may depend strongly on the mentioned parameters. A difficult problem in such complex systems is to determine, in general, what parameter combination induce which motion. This paper attacks this problem. Analytical results are obtained for the location in parameter space where quasiperiodic and synchronized states are generated in pairs of coupled maps. The generations of such quasiperiodic and synchronized states are related with a qualitative change in the motion of the particles of the system. Such changes may be modeled adequately by equations with solutions, which display NS bifurcations. After the NS bifurcation, a fixed-point solution is transformed into a limit-cycle with quasiperiodic motion. For very specific conditions, the fixed-point solution is transformed into a mode-locked or synchronized state.

This paper analyzed the above mentioned qualitative changes in the solutions for two maps, coupled asymmetrically and symmetrically. Such results were obtained using normal forms [24]. For each kind of coupling, coefficients of the normal forms (20) and (21) were determined along the stability boundaries for the quasiperiodic motion, called also the NS bifurcation lines [Eqs. (29), (41), and (50)]. The emergence of synchronized states (or mode-locked states) of *any* period, always embedded in the quasiperiodic motion, was found analytically in the parameter space. Such points of mode-locked states are the origin of Arnold tongues [4]. Analytical formulas obtained for the stability boundaries in parameter space [Eqs. (29), (41), and (50)], limit cycles and radius of the limit cycles in phase space [Eq. (33)], are in good agreement (within the local approximation) with numerical calculations.

Numerical results, including Lyapunov exponents, parameter space and phase space portraits, were used to describe the transition from synchronized and quasiperiodic states into chaotic states. Basically, as one moves away from the NS bifurcation lines, firstly the radius of the limit-cycles (elliptic form) increases until the elliptic shape starts to be deformed. Then, the deformed limit cycle solution folds more and more on itself until, relatively far away from the NS line, the chaotic state is reached. Such transition was observed in phase spaces [Figs. 4(a) and 7(b)], Lyapunov exponents and bifurcation diagrams (Figs. 3 and 8), and parameter space [Figs. 1 and 7(a)].

Appendix A

The parameters of the normal forms [Eqs. (20) and (21)] for the symmetric coupled maps [Eqs. (3) and (4)] are presented in this appendix. After straightforward calculations, we determine that

$$
\begin{aligned}
f(u,v) = &\left\{ \left[-b^3 - 15b^2 - 31b - 17 - 4b(b+4)\eta' \right] u^4 + \left\{ \left[2b^3 + 6b^2 - 2b - 6 + 4\eta^2\eta' \right]\eta \right\} u^3 \right. \\
&+ \left\{ b^5 - 2b^4 - 10b^3 - 2b^4 - 10b^3 - 4b^2 + 9b + 6 + \left(2b^4 + 6b^3 - 2b^2 - 6b \right)v \right. \\
&+ \left[-3b^3 - 5b^2 + 3b + 5 - 4bv\eta \right]\eta' \right\} u^2 + \left[2(-b^3 + b^2 + b - 1)b\eta \right] uv \\
&\left. + \left(-b^5 + 2b^4 - 2b^2 + b \right)v^2 \right\} / [(b-1)(b+1+\eta')\eta],
\end{aligned}
$$

$$
\begin{aligned}
g(u,v) = &\left\{ \eta^2 v^4 + \left[2\eta^2\eta' + 2(-b^3 - b^2 + b + 1) \right]v^3 + \left[2(-b^2 - b - b - \eta')u\eta b^4 - 3b^3 \right. \right. \\
&- b^2 + 3b + 2 + \left(-2b^3 - 3b^2 + 2b + 3 \right)\eta' \right]v^2 + \left\{ \left[-4(1+b)\eta' - 2b^2 - 8b - 6 \right]b\eta \right\}vu \\
&\left. + \left[\left(b^4 + 3b^3 - b^2 - 3b \right) - 2b\eta^2\eta' \right]u^2 \right\} / [(b+1)(b-1)],
\end{aligned}
$$

where $\eta' = \sqrt{2(b+1)}$. Functions $f(u,v)$ and $g(u,v)$ are used to determine the coefficient

$$
e = \frac{36b^4 + 210b^3 + 454b^2 + 430b + 150(6b^4 + 67b^3 + 209b^2 + 253b + 105)\eta'}{2(b-1)(b+1+\eta')^2},
$$

which is always negative for the interval $-1 < b < 1$, and therefore, the limit cycles which are born at the bifurcation line are stable. The last parameter is

$$
s = \frac{(4b^3 + 8b^2 - b - 3)(6b + b\eta' + 10 + 7\eta')(3b + 5)b\eta}{(b-1)^2(b+1+\eta')^2(1-4b^2)}.
$$

References

[1] Wiggins S. Introduction to applied nonlinear dynamical systems and chaos. New York: Springer-Verlag; 1990.
[2] While NS bifurcation are the transition from periodic to quasiperiodic motion, Hopf bifurcations (Hopf E. Ber Math-Phys Sächs Akad Wiss 1942;94:1) are the transition from stationary to periodic motion. There are many references of the appearance of Hopf bifurcations in realistic complex systems, but it is not the scope of this paper to review such works.
[3] Marques F, Lopez JM, Shen J. A periodically forced flow displaying symmetry breaking via a three-tori gluing bifurcation and two-tori resonances. Physica D 2001;156:81–97.
[4] Schuster HG. Deterministic chaos, an introduction. Weinheim: VCH; 1989.
[5] Mach R, Schweitzer F. Multi-agent model of biological swarming. Lec Not Art Intel, vol. 2801, 2003. p. 810–20.
[6] Avramov KV. Non-linear beam oscillations excited by lateral force at combination resonance. J Sound Vib 2002;25:337–59.
[7] Koto T. Periodic orbits in the Euler method for a class of delay differential equations. Comp Math App 2001;42:1597–608.
[8] Reimann S. Oscillation and pattern formation in a system of self-regulating cells. Physica D 1998;114:338–61.
[9] Neubert MG, Kot M. The subcritical collapse of predator populations in discrete-time predator–prey models. Math Biosci 1992;110:45–66.
[10] Brock WA, de Fontnouvelle P. Expectational diversity in monetary economies. J Econ Dyn Control 2000;24:725–59.
[11] Peng M. Multiple bifurcations and periodic ''bubbling'' in a delay population model. Chaos, Solitons & Fractals 2005;25:1123–30;
Coninck JCP, Lopes SR, Viana RL. Multistability and phase-space structure of dissipative nonlinear parametric four-wave interactions. Phys Rev E 2004;70:056403;
Bragard J, Boccaletti S, Mendoza C, Hentschel HGE, Mancini H. Synchronization of spatially extended chaotic systems in the presence of asymmetric coupling. Phys Rev E 2004;70:036219;
Baptista MS, Boccaletti S, Josic K, Leyva I. Irrational phase synchronization. Phys Rev E 2004;69:056228;
Neumann E, Sushko I, Maistrenko Y, Feudel U. Synchronization and desynchronization under the influence of quasiperiodic forcing. Phys Rev E 2003;67:026202;
Boccaletti S, Kurths J, Osipov G, Valladares DL, Zhou CS. The synchronization of chaotic systems. Phys Rep 2002;366:101;
Maistrenko YL, Maistrenko VL, Popovych O, Mosekilde E. Desynchronization of chaos in coupled logistic maps. Phys Rev E 1999;60:2817–30.
[12] Marin J, Sole RV. Controlling chaos in unidimensional maps using macroevolutionary algorithms. Phys Rev E 2002;65:026207;
Galias Z. Interval methods for rigorous investigations of periodic orbits. Int J Bif Chaos 2001;11:2427–50.
[13] Beims MW, Gallas JAC. Accumulation points in nonlinear parameter lattices. Physica A 1997;238:225–44;
Gallas JAC. Units: Remarkable points in dynamical systems. Physica A 1995;222:125–51.
[14] Endler A, Gallas JAC. Arithmetical signatures of the dynamics of the Hénon map. Phys Rev E 2002;60:036231.
[15] Endler A, Gallas JAC. Reductions and simplifications of orbital sums in a Hamiltonian repeller. Phys Lett A 2006;352:124–8.

[16] Gelfand IM, Kapranov MM, Zelevinsky AV. Discriminants, resultants, and multidimensional determinants. Basel: Birkhäuser; 1994.

[17] Gross T, Feudel U. Analytical search for bifurcation surfaces in parameter space. Physica D 2004;195:292–302;
Guckenheimer J, Myers M, Sturmfels B. Computing Hopf bifurcations. I SIAM J Numer Anal 1997;34:1–21;
Gallas JAC. Structure of the parameter space of a ring cavity. Appl Phys B 1995;60:S203–13. Festschrift Herbert Walther;
Gallas JAC. A method for studying stability domains in physical systems. Physica A 1994;211:57–83.

[18] Feigenbaum MJ. Universal metric properties of non-linear transformations. J Stat Phys 1979;21:669–706.

[19] Hunt BR, Gallas JAC, Grebogi C, Yorke JA, Koçak H. Bifurcation rigidity. Physica D 1999;129:35–56;
Ringland J, Schell M. Universal geometry in the parameter plane of dissipatice dynamic-systems. Europhys Lett 1990;12:595–601.

[20] Bonatto C, Garreau JC, Gallas JAC. Self-similarities in the frequency-amplitude space of a loss-modulated CO_2 laser. Phys Rev Lett 2005;95:143905.

[21] Gallas JAC. Degenerate routes to chaos. Phys Rev E 1993;48:R4156–9.

[22] Hartwich K, Fick E. Hopf bifurcations in the logistic map with oscillating memory. Phys Lett A 1993;177:305–10.

[23] Kürten KE, Nicolis G. Bifurcation scenarios and quasiperiodicity in coupled maps. Physica A 1997;245:446–52;
Reick C, Mosekilde E. Emergence of quasi-periodicity in symmetrically coupled, identical period-doubling systems. Phys Rev E 1995;52:1418–35;
Kook H, Ling FH, Schmidt G. Universal behavior of coupled nonlinear systems. Phys Rev A 1991;43:2700–8;
Hogg T, Huberman BA. Generic behavior of coupled oscillators. Phys Rev A 1984;29:275–81;
Frøyland J. Some symmetric, two-dimensional, dissipative maps. Physica D 1983;8:423–34.

[24] Guckenheimer J, Holmes P. Nonlinear oscillations, dynamical systems, and bifurcations of vector fields. New York: Springer-Verlag; 1986.

[25] Wan YH. Computation of stability condition for Hopf bifurcation of difeomorphisms on R2. SIAM J Appl Math 1978;34:167–75;
Iooss G, Joseph DD. Elementary stability and bifurcation theory. Heidelberg: Springer-Verlag; 1981.

[26] Yaghoobi H, Abed EH. Local feedback control of the Naimark–Sacker bifurcation. Int J Bif Chaos 2003;13:879–93.

[27] Gallas JAC. Structure of the parameter space of the Hénon map. Phys Rev Lett 1993;70:2714–7.

[28] Rech PC, Beims MW, Gallas JAC. Naimark–Sacker bifurcations in linearly coupled quadratic maps. Physica A 2004;342:351–5.